FEBS Open Bio 3 (2013) 218–224

journal homepage: www.elsevier.com/locate/febsopenbio

Zinc-binding and structural properties of the histidine-rich loop of *Arabidopsis thaliana* vacuolar membrane zinc transporter MTP1☆

Natsuki Tanaka[a], Miki Kawachi[a,b], Takashi Fujiwara[a], Masayoshi Maeshima[a,*]

[a]Laboratory of Cell Dynamics, Graduate School of Bioagricultural Sciences, Nagoya University, Nagoya 464-8601, Japan
[b]Institute for Advanced Research, Nagoya University, Nagoya 464-8601, Japan

ARTICLE INFO

Article history:
Received 18 March 2013
Received in revised form 17 April 2013
Accepted 17 April 2013

Keywords:
Circular dichroism spectroscopy
Histidine-rich loop
Isothermal titration calorimetry
Metal tolerance protein
Zinc binding
Zinc transporter

ABSTRACT

The vacuolar Zn^{2+}/H^{+} antiporter of *Arabidopsis thaliana*, AtMTP1, has a cytosolic histidine-rich loop (His-loop). We characterized the structures and Zn^{2+}-binding properties of the His-loop and other domains. Circular dichroism analyses revealed that the His-loop partly consists of a polyproline type II structure and that its conformational change is induced by Zn^{2+} as well as the C-terminal domain. Isothermal titration calorimetry of the His-loop revealed a binding number of four Zn^{2+} per molecule. Numbers of Ni and Co associated with the His-loop were approximately one ion per molecule and the thermodynamic parameters of the association with these ions were different from that of Zn^{2+}. These results suggest the involvement of the His-loop in sensing cytosolic Zn^{2+} and in the regulation of zinc transport activity through Zn^{2+}-induced structural change.

© 2013 The Authors. Published by Elsevier B.V. on behalf of Federation of European Biochemical Societies. All rights reserved.

1. Introduction

Metal tolerant protein 1, MTP1, belongs to the cation diffusion facilitator (CDF) family and functions as an active transporter. In addition to MTP family members, mammalian zinc transporters such as ZnT4 (SLC30A4) [1], *Saccharomyces cerevisiae* ZRC1 (ScZRC1) [2] and *Escherichia coli* YiiP [3] are also members of the same family. MTP1 proteins have six transmembrane (TM) domains, an N-terminal domain (NTD), and a C-terminal domain (CTD). NTD is exposed to the cytoplasm and CTD has metal-binding sites and protrudes into the cytoplasm as demonstrated for YiiP [4,5]. The CDF members transport Zn^{2+}, Cd^{2+}, Co^{2+}, and/or Ni^{2+} as a cation/H^{+} exchanger, although the ion selectivity varies with the molecular species [1–3,6,7]. For example, YiiP has the capacity to transport Zn^{2+}, Fe^{2+}, and Cd^{2+} [4]; ScZRC1 transports Zn^{2+} [2]; and ScCOT1 transports Zn^{2+}, Co^{2+}, and Cd^{2+} [8]. Structure-based ion selectivity has been reported for YiiP [4,5], AtMTP1 [9], and *Noccaea goesingense* MTP1 (NgMTP1, formerly *Thlaspi goesingense* MTP1) [10].

Arabidopsis thaliana AtMTP1 functions in the vacuolar membrane as a Zn^{2+}/H^{+} exchanger to sequester cytoplasmic Zn^{2+} with the help of vacuolar proton pumps [7,11,12]. Zinc accumulation in the vacuole has two physiological roles: reservation of Zn^{2+} as a key nutrient and detoxification of excess Zn^{2+} in the cytoplasm. Zinc is an essential micronutrient but is toxic at high concentrations [13–15]. The loss-of-function mutant *atmtp1* is phenotypically sensitive to excess Zn^{2+} in the medium, showing the importance of AtMTP1 in zinc homeostasis, particularly for detoxification of zinc in the cytoplasm [16,17]. Thus, the recognition or sensing of the cytoplasmic Zn^{2+} concentration by AtMTP1 is a key process in maintaining zinc homeostasis in cells.

AtMTP1 has a long, cytosolic histidine-rich loop (His-loop). Other MTPs such as *Arabidopsis halleri* MTP1, *N. goesingense* MTP1t1 (formerly TgMTP1t1), *Populus* MTP1, and ScCOT1 also have a His-loop although the number of histidine residues and the length of the loop differ among each [7,13]. Furthermore, a mutant of AtMTP1 that lacks the first half of the His-loop has enhanced Zn^{2+} transport activity [7]. Therefore, the His-loop of AtMTP1 is not essential for Zn^{2+} transport and is estimated to play roles as a buffering pocket for Zn^{2+} and as a sensor of Zn^{2+} levels [7].

Information on the tertiary structure and on the kinetic properties of Zn^{2+} binding of the His-loop is essential to understand the biochemical and structural role of the loop. The fine tertiary structure of the *E. coli* CDF member YiiP in a functional homodimer has been resolved [4,5]. YiiP has six TM domains and a common CTD but lacks the His-loop. Also, the primary structure of the NTD is different from that of AtMTP1. Thus, homology modeling cannot be applied to estimate the 3D structure of the His-loop. In this study, we prepared polypeptides of the His-loop and other domains, including NTD and CTD, to investigate their structures and Zn^{2+}-binding properties. We found

☆ This is an open-access article distributed under the terms of the Creative Commons Attribution License, which permits unrestricted use, distribution, and reproduction in any medium, provided the original author and source are credited.

Abbreviations: CTD, carboxyl terminal domain; His-loop, histidine-rich loop; ITC, isothermal titration calorimetry; MTP, metal tolerant protein; NTD, amino terminal domain; PPII, polyproline type II; TFE, trifluoroethanol; TM, transmembrane.

* Corresponding author. Tel.: +81 52 789 4096.
E-mail addresses: tanaka.natsuki@h.mbox.nagoya-u.ac.jp (N. Tanaka)
mkawachi@agr.nagoya-u.ac.jp (M. Kawachi) takafuji@agr.nagoya-u.ac.jp (T. Fujiwara)
maeshima@agr.nagoya-u.ac.jp (M. Maeshima).

2211-5463/$36.00 © 2013 The Authors. Published by Elsevier B.V. on behalf of Federation of European Biochemical Societies. All rights reserved.
http://dx.doi.org/10.1016/j.fob.2013.04.004

that the His-loop binds multiple Zn^{2+} ions and changes its secondary structure upon Zn^{2+} binding, and that the NTD has no capacity to bind Zn^{2+}. We discuss the biochemical relevance of the His-loop in the regulation of zinc transport activity and ion selectivity with these results.

2. Materials and methods

2.1. Plasmid construction and protein expression

To determine the physico-chemical properties using a large quantity of highly purified samples, we prepared recombinant polypeptides of NTD and CTD, and the second half of the His loop (His-loop 2nd half), which were tagged with $(His)_6$. Their cDNAs were prepared from a cDNA library by polymerase chain reaction (PCR) using the primer sets listed in Table S1. PCR was performed using KOD-Plus DNA polymerase (Toyobo, Osaka, Japan). The amplified DNA fragments were treated with restriction enzymes *Nde* I and *Eco* RI and then cloned into the vector pET23b (Novagen, Madison, WI, USA) for introduction into *E. coli* DH5α competent cells (Takara Bio, Otsu, Japan). All constructs were sequenced to verify the PCR errors, and then the expression vector was introduced into *E. coli* BL21(DE3) (Novagen). The transformants were grown in Luria–Bertani (LB) broth supplemented with 0.1 mg/ml ampicillin for 18 h at 25 °C for the NTD and the His-loop 2nd half, and for 8 h at 30 °C for CTD after induction with 0.5 mM isopropyl-1-thio-β-D-galactoside.

2.2. Purification of polypeptides

The transformed *E. coli* cells were harvested by centrifugation, resuspended in buffer, and then disrupted by sonication by the method described previously [18]. After removal of cell debris by centrifugation at 100,000*g* for 30 min, the supernatants were applied to a nickel nitrilotriacetic acid Superflow (Ni-affinity) column (1.5 × 12 cm) (Qiagen, Valencia, CA, USA) equilibrated with 20 mM Tris–acetate, pH 7.5, 20 mM imidazole, 20% (v/v) glycerol, and 2 M NaCl, and then washed with 20 mM Tris–acetate, pH 7.5, 20 mM imidazole, and 2 M NaCl. The recombinant proteins were eluted with 20 mM Tris–acetate, pH 7.5, 300 mM imidazole, and 2 M NaCl.

The obtained protein solutions were dialyzed overnight against 20 mM sodium phosphate, pH 7.0, and 150 mM NaCl (TAGZyme buffer) to remove imidazole. The His tag was removed by a TAGZyme kit (Qiagen) according to the manufacturer's manual. The recombinant proteins without a tag were separated from recombinant proteins with a tag by Ni-affinity column chromatography. Highly purified preparations of the CTD and the His-loop 2nd half were obtained after this step. Their purity was checked by SDS–polyacrylamide gel electrophoresis (PAGE) using precast 15% gels (Atto, Tokyo, Japan) in Tris–Tricine buffer.

NTD was further purified by gel filtration with Hiprep 16/60 Sephacryl S-100 HR (GE Healthcare, Piscataway, NJ, USA). The obtained solutions of the CTD and the His-loop 2nd half were subjected to dialysis to exchange the buffer. The polypeptide of the His-loop and its 1st half were synthesized chemically by Genscript-Japan (Tokyo, Japan) and Operon (Tokyo, Japan), respectively, because the polypeptides were not expressed at a high level in *E. coli*. Biochemical properties are listed in Table S2.

2.3. Circular dichroism spectroscopy

The ellipticity was followed with a J-700 spectropolarimeter equipped with a PTC-348 WI temperature controller (Jasco, Tokyo, Japan) at 25 °C [19]. Far-UV CD spectra of samples (0.4 ml) in 20 mM Tris–acetate, pH 7.5, were monitored in a range of 200–250 nm with a light path length of 1 mm in the presence or absence of $ZnSO_4$. All spectra are shown as the average of five scans. In some experiments, protein samples were dissolved in 10–50% (v/v) of trifluoroethanol (TFE). In all cases, the background signal for the buffer was subtracted from that of the sample spectra. The detailed measurement conditions are listed in Table S3.

The content of α helices (f_H) in a polypeptide was calculated with the following Eqs. (1) and (2),

$$[\theta]_{222} = \frac{[\theta]_{obs}}{(d \times c)} \tag{1}$$

$$f_H = \frac{([\theta]_{222} + 2340)}{30,300} \tag{2}$$

where $[\theta]_{222}$ represents the molar ellipticity at 222 nm, $[\theta]_{obs}$ the observed value of ellipticity (degree), d light path (m), and c amino acid molar concentration (M) [20].

2.4. Isothermal titration calorimetry

Isothermal titration calorimetric (ITC) analysis was performed using an isothermal titration calorimeter Nano-ITC LV (TA Instruments, New Castle, PA, USA). Protein samples in 20 mM Tris–acetate, pH 7.5, were diluted with the same buffer and degassed in a vacuum. Aliquots (2 or 3 μl) of 2 or 4 mM $ZnSO_4$ were injected into a 0.190 ml sample cell containing 0.2 mM (for His-loop), 0.4 mM (for the 1st half), and 0.15 mM (for the 2nd half) at 25 °C. The total volume of zinc solution was 50 μl. In all cases, the background titration signal for the buffer was subtracted from that of the sample spectra. The data were analyzed using NanoAnalyze (TA Instruments). The calculation was based on the assumption that each polypeptide has one set of identical binding sites for the metal ion. The detailed measurement conditions are listed in Table S4. The enthalpy change (ΔH), the association constant (K_a), and the stoichiometry (n) were determined using the ITC titration curve of the binding of Zn^{2+} to the corresponding protein, and the free-energy change (ΔG) and the entropy change (ΔS) on Zn^{2+} binding was then calculated with the following Eq. (3),

$$\Delta G = -RT \ln K_a = \Delta H - T\Delta S \tag{3}$$

where R represents the gas constant and T the absolute temperature.

3. Results

3.1. Preparation of polypeptides with domain sequences

A relatively large amount of proteins was prepared for biochemical analyses. The recombinant polypeptides of NTD (54 residues, Met-1 to Ser-54) (Fig. S1), CTD (79 residues, Met-320 to Arg-398), and the His-loop 2nd half (42 residues, Glu-217 to Asn-258) tagged with $(His)_6$ were well expressed in *E. coli*. After removal of the $(His)_6$ tag with exoprotease, these polypeptides were purified by affinity column chromatography and then gel filtration column chromatography. The obtained samples were pure as shown in SDS–PAGE (Fig. S2). The His-loop (77 residues, His-182 to Glu-251) and its 1st half (35 residues, His-182 to His-216) were chemically synthesized, because the expression levels in *E. coli* were not high. It should be noted that CTD shows a band at 16 kDa in addition to a monomer band of 8 kDa. The 16-kDa band is a homodimer of the CTD polypeptide. CTD has a single cysteine residue (Cys-362) and tends to form a dimer as shown in Fig. S2. The dimer formation is due to a disulfide bond between the monomers, because dimer formation was stimulated by Cu(II)-$(1,10\text{-phenanthroline})_3$, which is an oxidizing agent that stimulates the formation of disulfide bonds [21], and was cleaved by dithiothreitol (Fig. S3). The apparent molecular sizes on SDS–PAGE, the calculated molecular masses, and the p*I* values of the prepared polypeptides are summarized in Table S2.

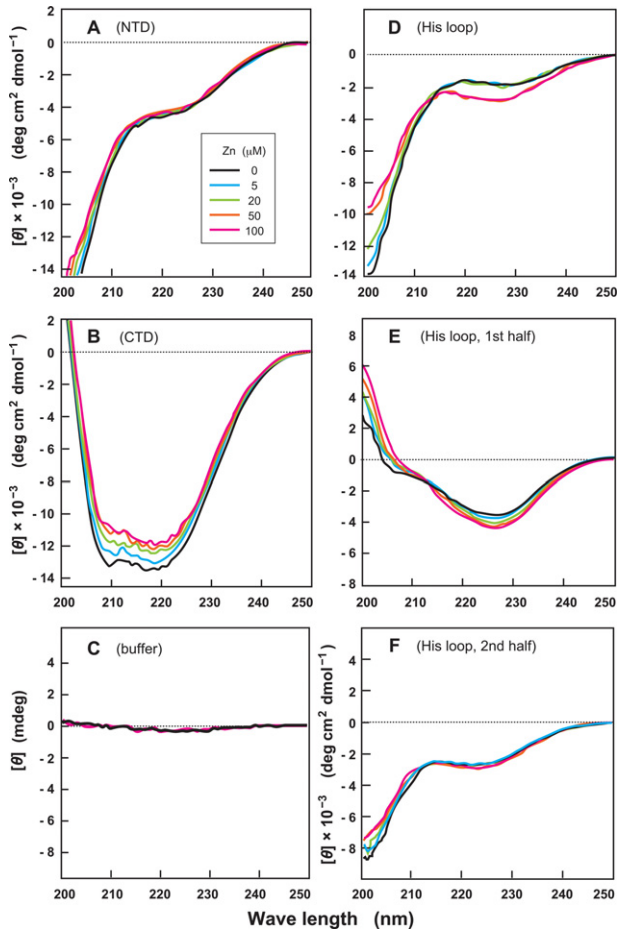

Fig. 1. Far-UV CD spectrum analysis of the secondary structures of the polypeptides and their spectral changes by Zn^{2+}. Purified preparations of NTD (A, 73 μg/ml), CTD (B, 77 μg/ml), His-loop (D, 200 μg/ml), His-loop 1st half (E, 200 μg/ml), and His-loop 2nd half (F, 102 μg/ml) in 20 mM Tris–acetate, pH 7.5, were subjected to far-UV CD spectral analysis. Panel C shows the spectrum of the buffer. The effect of the addition of Zn^{2+} at final concentrations of 5–100 μM was also examined. Detailed conditions are listed in Table S3.

3.2. *Secondary structures of the domains estimated by CD spectra*

We used CD spectroscopy to determine the secondary structures of polypeptides in solution. Each polypeptide showed a characteristic spectrum of far-UV CD as shown in Fig. 1. CTD was calculated to have an α-helix content of 34% (Fig. 1B), consistent with the 3D structure of the region estimated by homology modeling of AtMTP1 [9] with the crystal structure of *E. coli* YiiP [4,5]. By analysis using computational secondary structure prediction software (Parallel Protein Information Analysis system, PAPIA, http://mbs.cbrc.jp/papia/papiaJ.html), CTD was estimated to have an α-helix content of 43%, which was comparable to that from CD analysis.

The addition of Zn^{2+} changed the secondary structure of CTD. The helix content of CTD decreased from 34% to 28% at a final Zn^{2+} concentration of 100 μM. Although the results were obtained for the polypeptide of CTD, this change in the CD spectrum might reflect the conformational change of this region in the whole protein of MTP1 in response to Zn^{2+}-binding.

The tertiary structure of the AtMTP1 NTD could not be estimated due to the low sequence identity of the NTD between AtMTP1 and YiiP [9]. The computational prediction of the NTD with the PAPIA software revealed no helix, 19% β-conformation, and 81% random coil. In agreement with the prediction, the CD spectrum of NTD indicated a high content of random coil and a low content of α-helix (6%). The addition of Zn^{2+} did not change the secondary structure, suggesting no interaction with Zn^{2+} (Fig. 1A).

The His-loop is a unique sequence, which is absent in YiiP, and is thought to be a candidate for a regulatory domain of Zn^{2+} translocation and a sensory domain of the cytoplasmic Zn^{2+} level [7,9]. The CD spectrum indicated a low content of α-helix and high content of random conformation (Fig. 1D). The computational analysis with PAPIA software predicted 74% random conformation, 19% α-helix, and 7% β-conformation. Overall, the CD spectrum of the His-loop was similar to that of prothymosin α, which is a highly acidic polypeptide hormone of mammalian thymus [22,23]. The addition of Zn^{2+} at more than 50 μM decreased the ellipticity at 220–230 nm, suggesting a moderate increase in the contents of β-conformation and/or α-helix. No further change was detected at 100 μM Zn^{2+}. There is an isodichroic point at 212 nm, which means a linear combination of the structural transitions between the two conformational states.

In contrast to the whole His-loop, the CD spectrum of the His-loop 1st half indicated a relatively high content of β-conformation (Fig. 1E). A change in the spectrum by Zn^{2+} suggested a slight decrease in the random conformation and an increase in the contents in β-conformation and/or α-helix. The spectra of the 1st half indicated a slight increase in the contents of β-sheet and β-turn by Zn^{2+}, because the β-sheet and β-turn show a negative peak of the Cotton effect at 215–220 nm and at 225–230 nm, respectively [24]. On the other hand, the His-loop 2nd half had a relatively high content of random conformation as similar to the N-region and His-loop, and did not show any changes by addition of Zn^{2+} (Fig. 1F).

3.3. *Effect of heat and trifluoroethanol on the secondary structure of the His-loop*

Far-UV CD spectrum changes were measured at high temperatures to elucidate the temperature-dependent unfolding of the secondary structure of the His-loop. As temperature increased from 20 to 99 °C, the ellipticity at 220 nm gradually decreased with a concomitant increase in the intensity at 200 nm (Fig. 2A), and then gradually increased with a decrease in the temperature from 99 to 20 °C (Fig. 2B). In contrast, the value at 205 nm was maintained at a constant level of −8000 degree cm $dmol^{-1}$ in a wide range of temperatures, suggesting that there is an isodichroic point at 205 nm. The spectrum of the His-loop lacks the typical signatures of secondary structures of the α-helix and β-structure, except for a strong negative signal at 200 nm that is typically found in unstructured proteins [25]. A similar CD feature is found in many unstructured proteins, including the highly acidic protein, prothymosin α (calculated p*I*, 3.5) [22,23]. The difference CD spectra of the His-loop between 20 and 99 °C displayed a peak at 220 nm (Fig. 2C). The presence of a positive band at 220 nm indicated that the contribution of α-helical structure to the CD spectrum was absent or very low. These CD spectral features resemble those of peptides rich in polyproline type II (PPII) structures, like extended helices [25–27]. The PPII structure is observed frequently in proteins, even those with amino acids other than proline. The PPII content was calculated to be approximately 27% from the spectra with the assumption of absence of both α-helix and β-structure.

Trifluoroethanol (TFE) is known to stabilize the α-helical structures in proteins and small polypeptides [28,29]. The CD spectrum under normal conditions showed that the α-helix is absent in the His-loop. When TFE was added gradually, the molar ellipticity at around 215–225 nm decreased linearly as the TFE concentration increased (Fig. 2D), indicating an increase in α-helix content. The content of α-helix was calculated to be 25% at 50% TFE. The result suggests that the His-loop has the potential to form a tertiary structure with a relatively high α-helix content. The α-helix content was markedly decreased by high concentrations of Zn^{2+} in the presence of TFE at 50% (data not shown), suggesting that zinc disturbs the formation of α-helices in the His-loop.

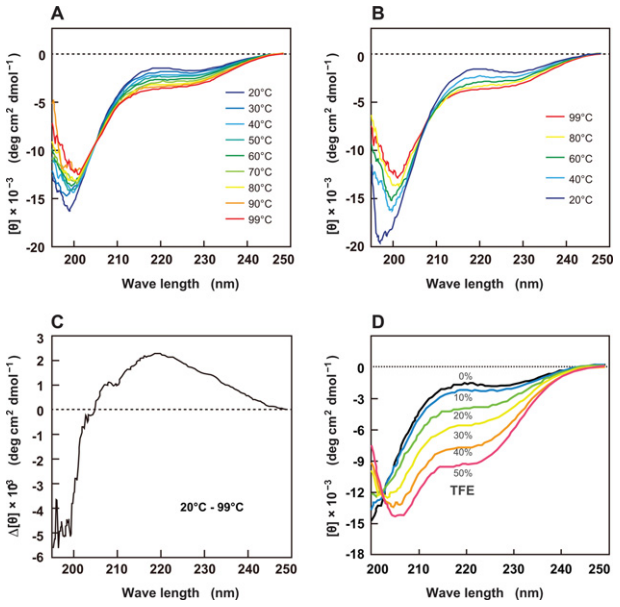

Fig. 2. Structural changes of the His-loop by heat and trifluoroethanol. (A) Far-UV CD spectra of the His-loop were obtained every 10 °C from 20 °C (blue line) to 99 °C (red). The apparent isodichroic point was at 205 nm. (B) Far-UV CD spectra of the His-loop were obtained every 20 °C from 99 °C (blue line) to 20 °C (red). In this experiment, the cuvette temperature was decreased to monitor structural recovery from the heat-denatured condition. (C) Difference spectrum of the His-loop between 20 and 99 °C (20 °C − 99 °C). (D) Far-UV CD spectra of the His-loop were monitored in the presence or absence of TFE (10–50%). (For interpretation of the references to color in this figure legend, the reader is referred to the web version of this article.)

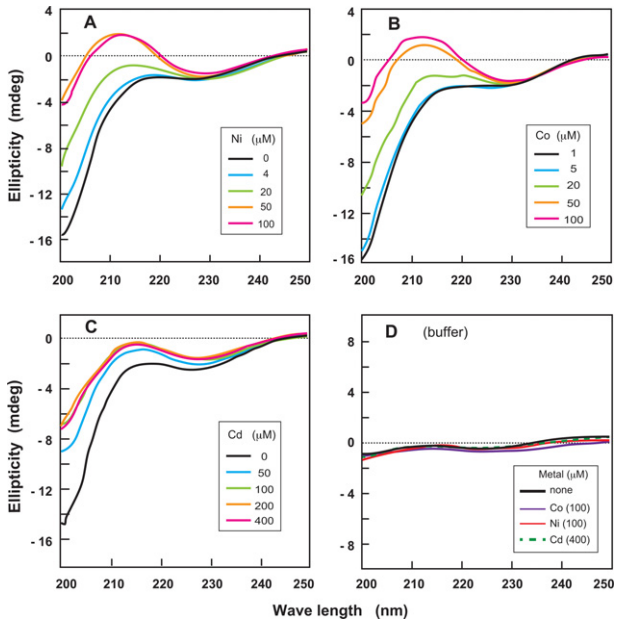

Fig. 3. Effect of metal ions on the structure of the His-loop. Far-UV CD spectra of the His-loop (25.7 μM) were monitored in the presence of Ni^{2+} (A), Co^{2+} (B), and Cd^{2+} (C) at indicated concentrations. The spectra of the buffer supplemented with the indicated metal ions were also monitored (D).

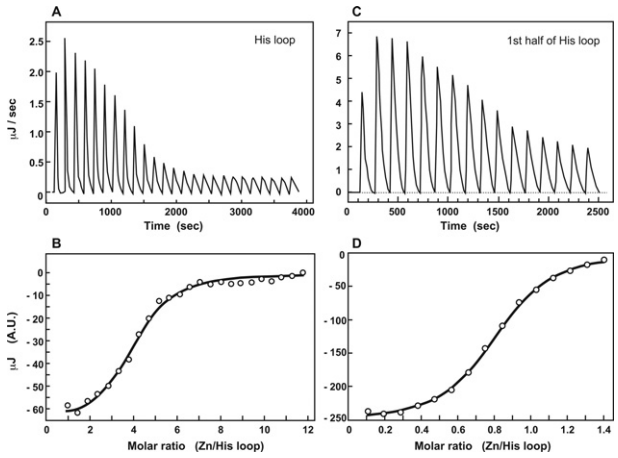

Fig. 4. Isothermal titration calorimetry for the association of Zn^{2+} with the His-loop and its 1st half. (A, C) Typical raw titration curves of the His-loop (A) and the His-loop 1st half (C) for Zn^{2+} binding monitored by ITC. (B, D) Integration of the thermogram yielded binding isotherm graphs of the His-loop (B) and the His-loop 1st half (D). The solid lines represent the non-linear regression of the data points according to a model of *n* identical binding sites with the same affinity and without allosteric effects to each site (see text for details). The parameters K_a (4.1×10^4 M^{-1}), *n* (4.0 ± 0.34), and ΔH (−9.89 kJ mol^{-1}) upon Zn^{2+} binding were obtained for the His-loop. The parameters K_a (8.3×10^4 M^{-1}), *n* (0.87 ± 0.058), and ΔH (−49.2 kJ mol^{-1}) upon Zn^{2+} binding were obtained for His-loop 1st half.

3.4. *Effect of other metals on the structure of the His-loop*

As nickel is known to bind His residues, the His-loop is estimated to have a high affinity to nickel. This point was examined by CD spectrum analysis in the presence of nickel and other metals at different concentrations (Fig. 3). Nickel changed the spectrum significantly at higher than 4 μM (Fig. 3A). The change was saturated at more than 50 μM. Cobalt showed a change in the spectrum at 20 μM (Fig. 3B). In both cases, the [θ] values at between 200 and 220 nm were increased and maximal peaks were observed at around 212 nm. The change by cadmium was smaller than that by nickel or cobalt (Fig. 3C).

3.5. *Zinc-binding kinetics of the His-loop determined by isothermal titration calorimetry*

CD analysis revealed that the polypeptides of the His-loop and the His-loop 1st half interact with Zn^{2+}. Then, we determined the binding parameters of the polypeptide–Zn^{2+} interaction by isothermal calorimetrical analysis. Both the His-loop and its 1st half gave clear titration curves of ITC (Fig. 4). From the curves, we calculated the thermodynamic parameters of metal binding on the basis of the assumption that each polypeptide has one set of identical binding sites for the metal ion. The binding-site number of Zn^{2+} to the His-loop was calculated to be approximately 4, and the association constant K_a was 41 ± 2.8 × 10^3 M^{-1} (Figs. 5 and 6, Table S5). The binding-site numbers of Ni^{2+}, Co^{2+}, and Cd^{2+} were approximately 1, 1, and 2, respectively. Among the four metals, the K_a value for Ni^{2+} was markedly higher, meaning a higher affinity of the His-loop for Ni^{2+}. The four metals showed similar ΔG values of the His-loop in a range from −23 to −30 kJ mol^{-1}. For Zn^{2+}, however, the contribution of the entropy ($-T\Delta S$) to ΔG was very large compared with Ni^{2+}, Co^{2+}, and Cd^{2+}.

Also, the His-loop 1st half was examined by ITC. Although the 1st half is rich in histidine residues (18 of 35 residues are histidine), the number of Zn^{2+}-binding sites and K_a were calculated to be approximately 1 and 83 ± 2.2 × 10^3 M^{-1}, respectively. The number of binding sites was approximately 1 each for Ni^{2+}, Co^{2+}, and Cd^{2+}.

4. Discussion

Crystallography is a powerful approach for understanding the functional tertiary structure of proteins. Indeed, the crystal structure of *E. coli* YiiP has provided information on its functional dimeric structure and dynamic change during its zinc transport motion [4,5]. AtMTP1, however, may not have a solvable crystal structure, because

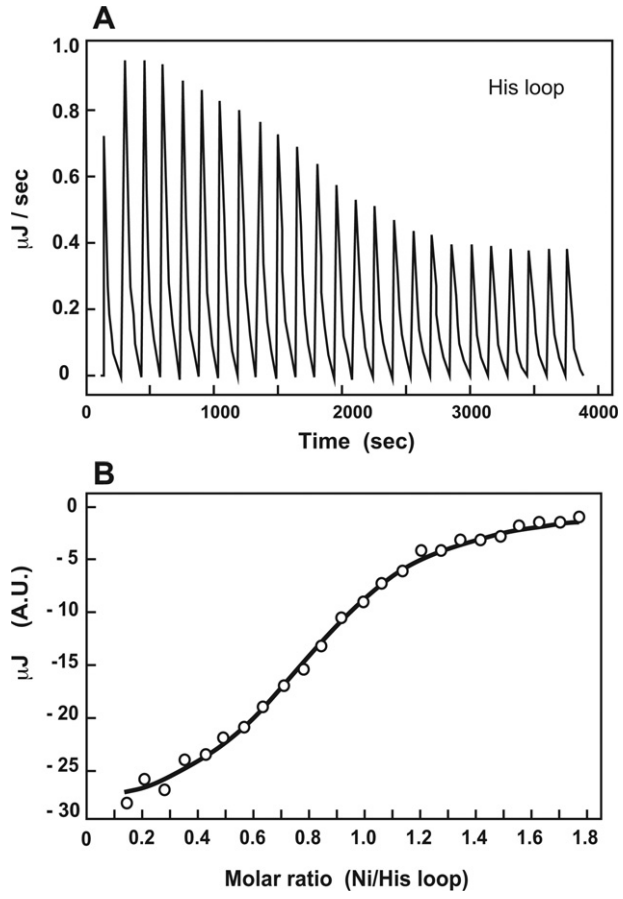

Fig. 5. Isothermal titration calorimetry for the association of Ni^{2+} with the His-loop. (A) Typical raw titration curve of the His-loop for Ni^{2+} binding monitored by ITC. (B) Integration of the thermogram yielded binding isotherm. The parameters K_a (2.5×10^5 M^{-1}), n (0.89 ± 0.10), and ΔH (−50.6 kJ mol^{-1}) upon Ni^{2+} binding were obtained for the His-loop.

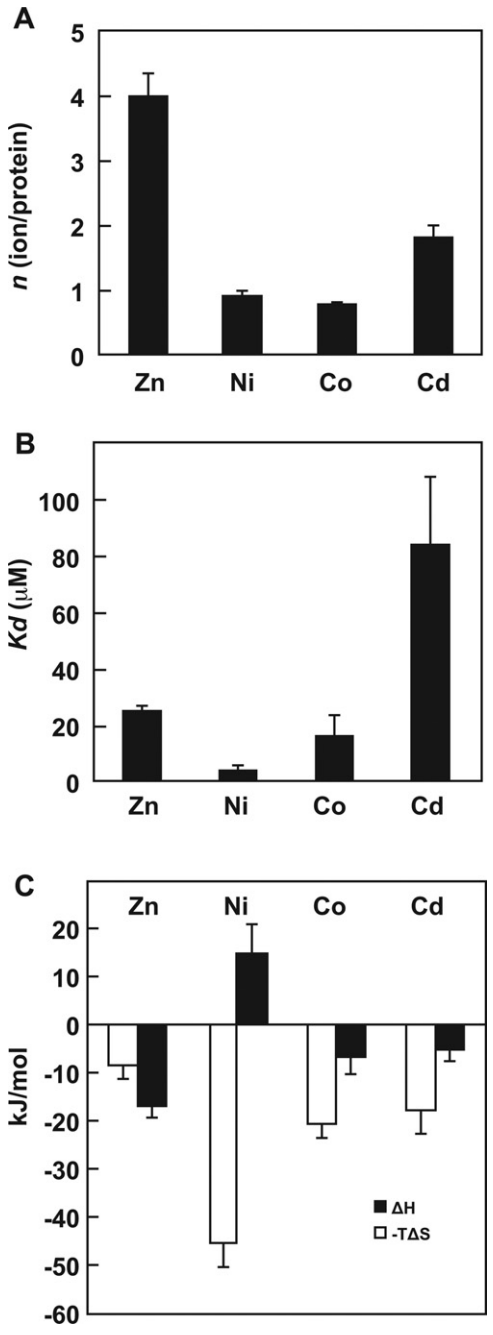

Fig. 6. Thermodynamic parameters of the binding of metal ions with the His-loop determined by ITC. The parameters n (A), K_d (B), and enthalpy (ΔH) and entropy energy ($-T\Delta S$) (C) of zinc, nickel, cobalt and cadmium ions were obtained for the His-loop.

proteins containing intrinsically disordered part(s) cannot form crystals. Here, we characterized five polypeptides, including the NTD and His-loop, by CD spectra and ITC analyses.

CTDs of the CDF members *E. coli* YiiP [4], *Thermus thermophilus* CzrB [30], and *Thermotoga maritima* TM0876 [31] have two α-helices and three β-strands. The crystal structures of YiiP and CzrB reveal a dynamic change in the interaction between the CTD of each monomer in the homodimer. In the zinc-binding forms of these transporters, the protomer is associated via Zn^{2+} binding and this rearrangement is tightly linked to the zinc transport mechanism [5,30]. From the 3D model of CTD, the difference in the secondary structure between the zinc-binding and free forms is estimated to be small. Considering the high sequence similarity of CTD, the CTD of AtMTP1 may include a rearrangement of CTD in the catalytic process. AtMTP1 showed a zinc-dependent conformational change (Fig. 1B); the α-helix content was decreased from 34% to 28% by zinc. The ellipticity at 200 nm was not changed by zinc, suggesting an increase in the content of β-conformation but not of random coil [20].

The α-helix contents of AtMTP1 CTD in the presence and absence of Zn^{2+} are comparable to those of bacterial CDF members. For example, the α-helix accounts for 32% of the CTD of *T. maritima* in the Zn^{2+}-free form (32 amino acid residues in the 101-residue domain). The contents of α-helix, β-strand, and random coil in CTD have been calculated to be 26%, 22%, and 52% from crystallography of the Zn^{2+}-binding form of *E. coli* YiiP [4]. The change in the α-helices in CTD was not as significant as in bacterial YiiP and CzrB as demonstrated previously [4,30], although the CTD orientation in the functional homodimer was dynamically changed by zinc binding [5].

The present study revealed that the His-loop has the capacity to bind four Zn^{2+} with a K_d of 25 μM. There are 25 histidine and no cysteine residues in the His-loop of 81 residues. The coordination number of Zn^{2+} is four or six and the low coordination number dominates. Generally, Zn^{2+} is coordinated by a domain with four amino acid residues, such as a H2C2 domain (a domain containing two histidine and two cysteine residues), in structural Zn sites of proteins [32,33]. In catalytic Zn sites, Zn^{2+} is coordinated by three amino acid residues and one exchangeable H_2O molecule, which is involved in the chemical reaction [33]. Considering the coordination number of Zn, 25 histidine residues in the His-loop might be enough to bind four

Zn^{2+} ions, although it is not clear whether the His-loop functions as a catalytic or a structural zinc site in AtMTP1. The zinc binding numbers of the 1st and 2nd halves of the His-loop are one and zero, respectively, suggesting that the individual half is not enough to form multiple zinc-binding sites. Thus, the four zinc-binding sites might be in the tertiary structure consisting of the 1st and 2nd halves of the His-loop.

The present study revealed a unique structure of the His-loop. From the CD spectra, the α-helix content was calculated to be almost zero. Furthermore, there was no typical signature of β-structure in the spectra. In our ^1H NMR analysis of the His-loop, there was no signal in the ^1H chemical shift at higher than 8.6 ppm in one-dimensional NMR spectrum (data not shown), meaning the absence of β-strand in the protein. The present study shows that the His-loop has no α-helices or β-strands but has the PPII structure, which is categorized as an intrinsically disordered structure. The content of the PPII structure was 27% at 20 °C and decreased to 19% in the presence of Zn^{2+} (Figs. 1D and 2). It should be noted that the His-loop formed α-helices in a solution containing TFE, a stabilizer of α-helices (Fig. 2D). The α-helix content of the loop in 50% TFE was 25%, which is comparable to the content of PPII under normal conditions. This indicates that the His-loop has the potential to form a helical structure in part. Thus, the His-loop might consist of approximately 30% PPII structure and 70% random coil. The CD analysis showed a slight decrease in the PPII structure by Zn^{2+}-binding. This might reflect the increase in entropy of the His-loop upon binding with Zn^{2+} (Table S5).

The ITC analysis demonstrated that the His-loop had the potential to bind four Zn^{2+} with a K_d value of 25 μM. This kinetic parameter might be reflected in the results of the CD analysis. The CD spectrum pattern of the His-loop was changed at more than 50 μM of Zn^{2+}, although no significant change occurred at lower than 20 μM (Fig. 1). The His-loop can be divided into the 1st and 2nd halves, which have 18 and 7 histidine residues, respectively (Fig. S1). The 1st, but not 2nd, half of the His-loop changed its conformation by Zn^{2+} (Fig. 1). Its zinc-binding number is approximately 1 with a K_d value of 12 μM (Fig. 4C and D; Table S5). These results indicate that the binding of four Zn^{2+} ions to the His-loop is achieved with coordination of the 1st and 2nd halves. In other words, each histidine-binding site consists of four histidine residues from both the 1st and 2nd halves.

These Zn-binding sites might be different from the Ni-binding sites. In the present study we obtained two results: first, the His-loop had the capacity to bind one Ni ion with a K_d of 4.0 μM (Table S5); second, the His-loop bound one Zn^{2+} ion even in the presence of 0.3 mM Ni^{2+} (Fig. S4). If the three Zn^{2+}-binding sites were free in the presence of Ni, the additional Zn^{2+}-binding number would be three. However, we obtained a binding number of approximately 1. These results suggest that the conformation at the Ni-binding state is different from that at the Zn-binding state. This is supported by the result that the CD spectrum of the loop with Ni^{2+} was clearly different from that with Zn^{2+} (Fig. 1D and Fig. 3A). The concentration of nickel in fresh water and soil is lower than that of zinc by two orders of magnitude [34]. Under physiological conditions, the concentration of nickel is lower than can be detected, as is that of Co^{2+} and Cd^{2+} [17,35], which also had the capacity to bind to the His-loop (Fig. 3, Table S5). AtMTP1 does not translocate Ni^{2+}, Co^{2+}, or Cd^{2+} as shown previously [6,7,13]. The binding of Ni^{2+}, Co^{2+}, or Cd^{2+} to the His-loop might suppress the Zn^{2+} transport activity of AtMTP1. Indeed, these three metals inhibit Zn accumulation into vacuoles of yeast expressing AtMTP1 [7]. With these observations, we speculate that Ni^{2+}, Co^{2+}, and Cd^{2+} bind to the His-loop, make an abnormal conformation of the loop, and finally inhibit the Zn^{2+} transport activity.

Finally, we should discuss the physiological role of the His-loop. The K_d value of the His-loop for Zn^{2+} obtained here (25 μM) was higher than the K_m of AtMTP1 Zn^{2+}-transport activity (0.3 μM) [7]. Also, a change in the CD spectrum of the His-loop was observed at a Zn^{2+} concentration of more than 20 μM. These results suggest that the His-loop recognizes an excessive concentration of Zn^{2+} at more than 20 μM in the cytosol and changes its conformation. Considering the previous observation that AtMTP1 without the His-loop 1st half expresses 11-fold activity of Zn^{2+} transport [7], there is a possibility that the His-loop suppresses the Zn^{2+} transport activity at low Zn^{2+} concentrations in the cytoplasm, and stimulates the activity at high concentrations to remove the toxicity of excess Zn^{2+}.

The present study clearly shows that the His-loop functions as the fourth Zn^{2+}-binding site in addition to the sites A, B, and C, which were shown for Yiip [4,5]. In the further step, this observation should be considered in the conformational change of whole AtMTP1. At present, the NTD and His-loop hardly form crystals because they have intrinsically disordered structures. The tertiary structure of AtMTP1 and dynamic conformational changes of whole protein, including domain–domain interaction, by low and high concentrations of Zn^{2+} remain to be resolved.

Acknowledgments

We thank Shin Kawano and Toshiya Endo (Graduate School of Science, Nagoya University) for supporting the ITC analysis, Yasuo Sugiyama (the Research Center for the Genetics, Nagoya University) for supporting the CD spectral analysis, and Mitsuhiro Takeda and Youhei Miyanoiri (the Structural Biology Research Center, Nagoya University) for supporting the NMR analysis and for helpful advice.

This work was supported by Grants-in-Aid from the Japan Society for the Promotion of Science (Grants 23248017 and 23657031), the Salt Science Foundation (1223), and the Steel Foundation for Environmental Protection Technology (2010-29) to M.M. And N.T. is financially supported as an excellent graduate student by the grants of Program for Leading Graduate Schools from the JSPS.

Supplementary material

Supplementary material associated with this article can be found, in the online version, at doi:10.1016/j.fob.2013.04.004.

References

[1] Küry S., Dreno B., Bezieau S., Giraudet S., Kharfi M., Kamoun R. (2002) Identification of *SLC39A4*, a gene involved in acrodermatitis enteropathica. Nat. Genet. 31, 239–240.
[2] MacDiarmid C.W., Milanick M.A., Eide D.J. (2002) Biochemical properties of vacuolar zinc transport systems of *Saccharomyces cerevisiae*. J. Biol. Chem. 277, 39187–39194.
[3] Chao Y., Fu D. (2004) Kinetic study of the antiport mechanism of an *Escherichia coli* zinc transporter, ZitB. J. Biol. Chem. 279, 12043–12050.
[4] Lu M., Fu D. (2007) Structure of the zinc transporter YiiP. Science 317, 1746–1748.
[5] Lu M., Chai J., Fu D. (2009) Structural basis for autoregulation of the zinc transporter YiiP. Nat. Struct. Mol. Biol. 16, 1063–1068.
[6] Krämer U. (2005) MTP1 mops up excess zinc in *Arabidopsis* cells. Trends Plant Sci. 10, 313–315.
[7] Kawachi M., Kobae Y., Mimura T., Maeshima M. (2008) Deletion of a histidine-rich loop of AtMTP1, a vacuolar Zn^{2+}/H^+ antiporter of *Arabidopsis thaliana*, stimulates the transport activity. J. Biol. Chem. 283, 8374–8383.
[8] Lin H.L., Kumanovics A., Nelson J.M., Warner D.E., Ward D.M., Kaplan J. (2008) Single amino acid change in the yeast vacuolar metal transporters Zrc1 and Cot1 alters their substrate specificity. J. Biol. Chem. 283, 33865–33873.
[9] Kawachi M., Kobae Y., Kogawa S., Mimura T., Krämer U., Maeshima M. (2012) Amino acid screening based on structural modeling identifies critical residues for the function, ion selectivity and structure of *Arabidopsis* MTP1. FEBS J. 279, 2339–2356.
[10] Persans M.W., Nieman K., Salt D.E. (2001) Functional activity and role of cation-efflux family members in Ni hyperaccumulation in *Thlaspi goesingense*. Proc. Natl. Acad. Sci. USA 98, 9995–10000.
[11] Desbrosses-Fonrouge A.G., Voigt K., Schroder A., Arrivault S., Thomine S., Kramer U. (2005) *Arabidopsis thaliana* MTP1 is a Zn transporter in the vacuolar membrane which mediates Zn detoxification and drives leaf Zn accumulation. FEBS Lett. 579, 4165–4174.

[12] Martinoia E., Maeshima M., Neuhaus E. (2007) Vacuolar transporters and their essential role in plant metabolism. J. Exp. Bot. 58, 83–102.
[13] Krämer U. (2010) Metal hyperaccumulation in plants. Annu. Rev. Plant Biol. 61, 517–534.
[14] Rogers E.E., Eide D.J., Guerinot M.L. (2000) Altered selectivity in an *Arabidopsis* metal transporter. Proc. Natl. Acad. Sci. USA 97, 12356–12360.
[15] Fukao Y., Ferjani A., Tomioka R., Nagasaki N., Kurata R., Nishimori Y. (2011) The iTRAQ analysis reveals mechanisms of growth defects due to excess zinc in *Arabidopsis thaliana*. Plant. Physiol. 155, 1893–1907.
[16] Kobae Y., Uemura T., Sato M.H., Ohnishi M., Mimura T., Nakagawa T. (2004) Zinc transporter of *Arabidopsis thaliana* AtMTP1 is localized to vacuolar membranes and implicated in zinc homeostasis. Plant Cell Physiol. 45, 1749–1758.
[17] Kawachi M., Kobae Y., Mori H., Tomioka R., Lee Y., Maeshima M. (2009) A mutant strain *Arabidopsis thaliana* that lacks vacuolar membrane zinc transporter MTP1 revealed the latent tolerance to excessive zinc. Plant Cell Physiol. 50, 1156–1170.
[18] Nagasaki N., Tomioka R., Maeshima M. (2008) A hydrophilic cation-binding protein of *Arabidopsis thaliana*, AtPCaP1, is localized to plasma membrane via *N*-myristoylation and interacts with calmodulin and the phosphatidylinositol phosphates, PtdIns(3,4,5)P_3 and PtdIns(3,5)P_2. FEBS J. 275, 2267–2282.
[19] Nagasaki-Takeuchi N., Miyano M., Maeshima M. (2008) A plasma membrane-associated protein of *Arabidopsis thaliana* AtPCaP1 binds copper ions and changes its higher order structure. J. Biochem. 144, 487–497.
[20] Chen Y.H., Yang J.T., Martinez H.M. (1972) Determination of the secondary structures of proteins by circular dichroism and optical rotatory dispersion. Biochemistry 11, 4120–4131.
[21] Mimura H., Nakanishi Y., Maeshima M. (2005) Disulfide bond formation in the H^+-pyrophosphatase of *Streptomyces coelicolor* and its implication in redox control and structure. FEBS Lett. 579, 3625–3631.
[22] Uversky V.N., Gillespie J.R., Millett I.S., Khodyakova A.V., Vasilenko R.N., Vasiliev A.M. (2000) Zn^{2+}-mediated structure formation and compaction of the "natively unfolded" human prothymosin α. Biochem. Biophys. Res. Commun. 267, 663–668.
[23] Chichkova N.V., Evstafieva A.G., Lyakhov I.G., Tsvetkov A.S., Smirnova T.A., Karapetian R.N. (2000) Divalent metal cation binding properties of human prothymosin α. Eur. J. Biochem. 267, 4745–4752.
[24] Nakanishi K., Berova N., Woody R.W. (1994) Circular Dichroism: Principles and Applications. Wiley-VCH Verlag GmbH.
[25] Park S.H., Shalongo W., Stellwagen E. (1997) The role of PPII conformations in the calculation of peptide fractional helix content. Protein Sci. 6, 1694–1700.
[26] Soulages J.L., Kim K., Arrese E.L., Walters C., Cushman J.C. (2003) Conformation of a group 2 late embryogenesis abundant protein from soybean. Evidence of poly(L-proline)-type II structure. Plant Physiol. 131, 963–975.
[27] Shi Z., Woody R.W., Kallenbach N.R. (2002) Is polyproline II a major backbone conformation in unfolded proteins? Adv. Protein Chem. 62, 163–240.
[28] Shiraki K., Nishikawa K., Goto Y. (1995) Trifluoroethanol-induced stabilization of the α-helical structure of β-lactoglobulin: implication for non-hierarchical protein folding. J. Mol. Biol. 245, 180–194.
[29] Anderson V.L., Ralall T.F., Rospigliosi C.C., Webb W.W., Eliezer D. (2010) Identification of a helical intermediate in trifluoroethanol-induced alpha-synuclein aggregation. Proc. Natl. Acad. Sci. USA 107, 18850–18855.
[30] Cherezov V., Hofer N., Szebenyi D.M.E., Kolaj O., Wall J.G., Gillilan R. (2008) Insights into the mode of action of a putative zinc transporter CzrB in *Thermus thermophilus*. Structure 16, 1378–1388.
[31] Higuchi T., Hattori M., Tanaka Y., Ishitani R., Nureki O. (2009) Crystal structure of the cytosolic domain of the cation diffusion facilitator family protein. Prot. Struct. Funct. Bioinf. 76, 768–771.
[32] Grossoehme N.E., Akllesh S., Guerinot M.L., Wilcox D.E. (2006) Metal-binding thermodynamics of the Histidine-rich sequence from the metal-transport protein IRT1 of *Arabidopsis thaliana*. Inorg. Chem. 45, 8500–8508.
[33] Atkins P., Overton T., Rourke J., Weller M., Armstrong F. (2010) Sriver & Atkins' Inorganic Chemistry. 5th ed. Oxford, UK: Oxford University Press.
[34] Greger M. (2004) Metal availability, uptake, transport and accumulation in plants. In: M.N.V. Prasad (Ed.), Heavy Metal Stress in Plants: From Biomolecules to Ecosystems. 2nd ed. Berlin Heidelberg: Springer-Verlag, pp. 1–27.
[35] Shaw B.P., Sahu S.K., Mishara R.K. (2004) Heavy metal induced oxidative damage in terrestrial plants. In: M.N.V. Prasad (Ed.), Heavy Metal Stress in Plants: From Biomolecules to Ecosystems. 2nd ed. Berlin, Heidelberg: Springer-Verlag, pp. 84–126.